OCTOBER 1981

PPPL-1838
UC-20G

GYROKINETIC APPROACH IN PARTICLE SIMULATION

BY

W. W. LEE

PLASMA PHYSICS LABORATORY

PRINCETON UNIVERSITY
PRINCETON, NEW JERSEY

This work was supported by the U.S. Department of Energy Contract No. DE-AC02-76-CHO 3073. Reproduction, translation, publication, use and disposal, in whole or in part, by or for the United States government is permitted.

"Gyrokinetic Approach in Particle Simulation"

W. W. Lee

Plasma Physics Laboratory, Princeton University

Princeton, N.J. 08544

Abstract

A new scheme for particle simulation based on the gyrophase-averaged Vlasov equation has been developed. It is suitable for studying low-frequency microinstabilities and the associated anomalous transport in magnetically confined plasmas. The scheme retains the gyroradius effects but not the gyromotion; it is, therefore, far more efficient and versatile than the conventional ones. Furthermore, the reduced Vlasov equation is also amenable to analytical studies.

I. Introduction

Gyrokinetic approach has been widely used in recent years for studying low-frequency microinstabilities in a magnetically confined plasma since its inception more than a decade ago.[1,2] It employs the gyrokinetic ordering that the characteristic frequencies of the waves and gyroradii are small compared to the gyrofrequencies and unperturbed scale lengths, respectively, and perturbed parallel scale lengths are of the order of unperturbed scale lengths. Such an ordering enables one to be rid of the explicit dependence on the phase angle of the Vlasov equation through gyrophase-averaging while retaining the gyroradius effects to the arbitrary value of the gyroradius over the perpendicular scale length. Finite gyroradius effects, as we know, are essential for many microinstabilities of interest in magnetic confinement devices such as tokamaks . Contrary to the original approach, Catto[3] has recently developed a gyrokinetic technique which first transforms the particle variables to the guiding center variables in the Vlasov equation before performing the gyrophase-averaging. The purpose of it is to obtain finite gyroradius effects in a more convenient manner for arbitrary magnetic fields. As it turns out, this technique of gyrokinetic change of variables also provides a starting point for the development of the particle simulation scheme reported here.

Particle code simulation has long been recognized as a useful tool for understanding nonlinear plasma behavior and has contributed significantly in this regard over the years. In the area of microinstabilities in tokamaks, the excitation of the convective cells due to unstable drift waves[4] and the magnetic field line reconnection caused by shear-Alfven waves[5] are just two examples. However, not unlike other numerical schemes, particle code

simulation also has its share of limitations. For conventional codes which operate on the first principles of Newtonian dynamics, the time step for particle pushing is limited by the highest characteristic frequency in the plasma, which can be several orders of magnitude larger than the frequency of interest. It is, therefore, rather inefficient, if possible at all, to simulate low-frequency phenomena with such a code. Efforts have been made in the past to eliminate high frequency oscillations in the simulation plasma. For example, drift-kinetic approximation for electrons has been made in the codes used for the investigations in Refs. 4 and 5.[6,7,8] However, the lower hybrid oscillation, which represents the highest frequency in the plasma for such cases, is still much larger than the frequency of interest. In this paper, we will present a particle simulation scheme which keeps finite gyroradius effects that are vital to the physics at hand, but, at the same time, eliminates the oscillations associated with particle gyromotion. Henceforth, particle pushing can be accomplished in the time scale of the low-frequency microinstabilities. The scheme is, therefore, most suitable for the simulation of tokamak plasmas.

Recently, long-time-step particle simulation has also been tackled on a different front. Several implicit schemes have been developed, in which the high-frequency oscillations are filtered out through numerical methods.[9,10,11] They represent a basic difference in philosophy than the scheme discussed in this paper as well as those in Refs. 6 and 8, in which the elimination of high-frequency oscillations is contingent upon the underlying physics. Although the implicit schemes are more general in nature, their applicability to two and three-dimensional tokamak plasmas has yet to be demonstrated.

In the present paper, the focus is on the development of an electrostatic

particle simulation scheme in the slab geometry. The scheme is accurate linearly for arbitrary values of $k_\perp \rho_i$, where ρ_i is the ion gyroradius. Nonlinearly, it is valid for $k_\perp \rho_i < 1$. The two-and-one-half-dimensional (x,y,v_x,v_y,v_z) simulation results from the present scheme agree very well in every aspect of the instability with those obtained earlier using particle ions and guiding center electrons.[12,13] In addition to the use of longer time-steps for particle pushing, the scheme also can afford to use fewer particles to study weaker instabilities because the numerical noise associated with the particle gyration is no longer a problem. Therefore, it represents a tremendous saving in computing resources. Since the procedures described here is rather general, they can be used easily to obtain the electrostatic and electromagnetic (low- β) versions of the scheme in the toroidal geometry. In view of the recent development of the multiple-scale particle simulation model,[14] in which the plasma equilibrium scale lengths are separated from the perturbation scale lengths, it is now possible to simulate fully three-dimensional steady-state plasma turbulence in the toroidal geometry with the present generation of computers. This paper represents the first step toward that direction.

The paper is organized as follows. In Sec. II, the basic formulation of the gyrokinetic equation in general geometry is presented. The procedures for the development of electrostatic particle simulation scheme in the slab geometry is discussed in detail in Sec. III. The particle pushing algorithm and the simulation results are given in Sec. IV, together with their comparisons with previous particle code results. Conclusions and recommendations for future work are given in Sec. V.

II. Basic Formulation

Let us first apply Catto's gyrokinetic change of variables[3] from $\underset{\sim}{x}$, $\underset{\sim}{v}$ to $\underset{\sim}{R}$, μ, $v_\parallel$, ϕ to the Vlasov equation in general geometry,

$$\frac{\partial F}{\partial t} + \left[\underset{\sim}{v}_\parallel + \frac{q}{m} \frac{\underset{\sim}{E} \times \hat{\underset{\sim}{b}}}{\Omega} \right] \cdot \frac{\partial F}{\partial \underset{\sim}{R}} - \Omega \frac{\partial F}{\partial \phi}$$

$$+ \underset{\sim}{v} \cdot \left[\left(\frac{\partial \underset{\sim}{\rho}}{\partial \underset{\sim}{x}} \right) \cdot \frac{\partial F}{\partial \underset{\sim}{R}} + \frac{\partial \mu}{\partial \underset{\sim}{x}} \frac{\partial F}{\partial \mu} + \frac{\partial v_\parallel}{\partial \underset{\sim}{x}} \frac{\partial F}{\partial v_\parallel} + \frac{\partial \phi}{\partial \underset{\sim}{x}} \frac{\partial F}{\partial \phi} \right]$$

$$+ \frac{q}{m} \underset{\sim}{E} \cdot \left[\frac{\underset{\sim}{v}_\perp}{B} \frac{\partial F}{\partial \mu} + \hat{\underset{\sim}{b}} \frac{\partial F}{\partial v_\parallel} + \frac{\hat{\underset{\sim}{b}} \times \underset{\sim}{v}_\perp}{v_\perp^2} \frac{\partial F}{\partial \phi} \right] = 0 \qquad (1)$$

where $F(\underset{\sim}{R}, \mu, v_\parallel, \phi, t)$ is the distribution function, $\underset{\sim}{E}(\underset{\sim}{x})$ is the perturbed electric field, $B(\underset{\sim}{x}) = |\underset{\sim}{B}|$ and $\hat{\underset{\sim}{b}}(\underset{\sim}{x}) = \underset{\sim}{B}/B$ where B is the total magnetic field, $\mu = v_\perp^2/2B$, $\underset{\sim}{\rho} = \underset{\sim}{v}_\perp \times \hat{\underset{\sim}{b}} / \Omega$, $\Omega = qB/mc$. $\underset{\sim}{v}_\perp = v_\perp(\cos\phi\, \hat{\underset{\sim}{e}}_1 + \sin\phi\, \hat{\underset{\sim}{e}}_2)$, $\underset{\sim}{v}_\parallel = v_\parallel \hat{\underset{\sim}{b}}$, $\hat{\underset{\sim}{b}} = \hat{\underset{\sim}{e}}_1 \times \hat{\underset{\sim}{e}}_2$, $\underset{\sim}{R} = \underset{\sim}{x} + \underset{\sim}{\rho}$, and

$$\frac{\partial \mu}{\partial \underset{\sim}{x}} = -\frac{\mu}{B} \frac{\partial B}{\partial \underset{\sim}{x}} - \frac{v_\parallel}{B} \left(\frac{\partial \hat{\underset{\sim}{b}}}{\partial \underset{\sim}{x}} \right) \cdot \underset{\sim}{v}_\perp \ ,$$

$$\frac{\partial v_\parallel}{\partial \underset{\sim}{x}} = \left(\frac{\partial \hat{\underset{\sim}{b}}}{\partial \underset{\sim}{x}} \right) \cdot \underset{\sim}{v}_\perp \ ,$$

$$\frac{\partial \phi}{\partial \underset{\sim}{x}} = \frac{v_\parallel}{v_\perp^2} \left(\frac{\partial \hat{\underset{\sim}{b}}}{\partial \underset{\sim}{x}} \right) \cdot \left(\underset{\sim}{v}_\perp \times \hat{\underset{\sim}{b}} \right) + \left(\frac{\partial \hat{\underset{\sim}{e}}_2}{\partial \underset{\sim}{x}} \right) \cdot \hat{\underset{\sim}{e}}_1 \ .$$

For a low-β (= plasma pressure/magnetic pressure) plasma, the electric field is given by

$$\underset{\sim}{E} = -\frac{\partial \Phi}{\partial \underset{\sim}{x}} - \frac{1}{c} \frac{\partial \underset{\sim}{A}_\parallel}{\partial t} \ . \qquad (2)$$

where $\Phi(\underset{\sim}{x})$ is the electrostatic potential and $\underset{\sim}{A}_{\parallel}(\underset{\sim}{x})$ is the parallel vector potential. Invoking the gyrokinetic ordering of $\omega/\Omega \sim \epsilon$, $\rho/L \sim \epsilon$, and $L \sim L_{\parallel}$ where ϵ is a smallness parameter, ρ the gyroradius, L the equilibrium scale length and $L_{\parallel}$ the perturbed parallel scale length, one can write down the lowest order equation of Eq. (1) as

$$-\frac{\partial F}{\partial \phi} = 0 \quad , \tag{3}$$

Here the perturbed fields are also considered to be $O(\epsilon)$. With

$$F = f + \epsilon\, g(\phi) \quad , \tag{4}$$

where f is the solution of Eq. (3) and is independent of phase ϕ, Eq. (1) to the next order reduces to

$$\frac{\partial f}{\partial t} + \left[v_{\parallel} + \frac{q}{m} \frac{\underset{\sim}{b} \times \hat{\underset{\sim}{b}}}{\Omega} \right] \cdot \frac{\partial f}{\partial \underset{\sim}{R}} - 0 \frac{\partial}{\partial \phi} \left[g - \frac{q}{m} \frac{\bar{\Phi}}{B} \frac{\partial f}{\partial \mu} \right]$$

$$+ \underset{\sim}{v} \cdot \left(\frac{\partial \underset{\sim}{B}}{\partial \underset{\sim}{x}} \right) \cdot \frac{\partial f}{\partial \underset{\sim}{R}} + \frac{\partial \mu}{\partial \underset{\sim}{x}} \frac{\partial f}{\partial \mu} + \frac{\partial v_{\parallel}}{\partial \underset{\sim}{x}} \frac{\partial f}{\partial v_{\parallel}} \Big] + \frac{q}{m} \underset{\sim}{E} \cdot \hat{\underset{\sim}{b}} \frac{\partial f}{\partial v_{\parallel}} = 0 \quad . \tag{5}$$

Note that the relations of

$$\frac{\partial \bar{\Phi}}{\partial \underset{\sim}{x}} = \frac{\partial \bar{\Phi}}{\partial \underset{\sim}{R}} \quad , \tag{6}$$

which is correct to the order ϵ, and

$$0 \frac{\partial \bar{\Phi}}{\partial \phi} = - \underset{\sim}{v}_{\perp} \cdot \frac{\partial \bar{\Phi}}{\partial \underset{\sim}{R}} \tag{7}$$

have been used in arriving at Eq. (5). By assuming that all the field quantities are independent of ϕ and by taking the gyrophase average of Eq. (5), we then recover the usual drift-kinetic equation

$$\frac{\partial f}{\partial t} + \left[\underset{\sim}{v}_{\ell} + \underset{\sim}{v}_{d} + \frac{q}{m} \frac{\underset{\sim}{E} \times \hat{\underset{\sim}{b}}}{\Omega} \right] \cdot \frac{\partial f}{\partial \underset{\sim}{R}} + \left[a_{\parallel} + \frac{q}{m} \underset{\sim}{E} \cdot \hat{\underset{\sim}{b}} \right] \frac{\partial f}{\partial v_{\parallel}} = 0 \quad , \tag{8}$$

where

$$\underset{\sim}{v}_{d} = \frac{1}{2\pi} \oint \underset{\sim}{v} \cdot \left(\frac{\partial \underset{\sim}{\rho}}{\partial \underset{\sim}{x}} \right) d\phi = \hat{\underset{\sim}{b}} \times \left[\frac{v_{\parallel}^2}{\Omega} \left(\hat{\underset{\sim}{b}} \cdot \frac{\partial}{\partial \underset{\sim}{x}} \right) \hat{\underset{\sim}{b}} + \frac{v_{\perp}^2}{2\Omega} \frac{\partial \ell n B}{\partial \underset{\sim}{x}} \right]$$

$$a_{\parallel} = \frac{1}{2\pi} \oint \underset{\sim}{v} \cdot \frac{\partial v_{\parallel}}{\partial \underset{\sim}{x}} d\phi = - \frac{v_{\perp}^2}{2} \left(\hat{\underset{\sim}{b}} \cdot \frac{\partial \ell n B}{\partial \underset{\sim}{x}} \right)$$

are the curvature and ∇B drifts and the parallel acceleration, respectively. The parallel drift is ignored in Eq. (8) because it is higher order in ϵ,[3] and $\oint \underset{\sim}{v} \cdot \left(\partial \mu / \partial \underset{\sim}{x} \right) d\phi = 0$. It should be mentioned here that, together with Eq. (2) and

$$\mu = v_{\perp}^2 / 2B = \text{constant},$$

Eq. (8) can be used for particle pushing for electrons for a low-β plasma in the general geometry. If we now assume that f is the part of the distribution function which can be described by the drift-kinetic equation, Eq. (5) then indicates that $g = (q/m)\,(\Phi/B)\,(\partial f/\partial \mu)$ which gives

$$F = f + \frac{q}{m} \frac{\Phi}{B} \frac{\partial f}{\partial \mu} \quad . \tag{9}$$

Substituting Eq. (9) into Eq. (1), and using again Eqs. (6) and (7) together

with

$$\frac{\partial \bar{\Phi}}{\partial v_\parallel} = 0 \ , \quad \frac{\partial \bar{\Phi}}{\partial \mu} = - \frac{B}{v_\parallel^2} \rho \cdot \frac{\partial \bar{\Phi}}{\partial \underset{\sim}{R}} \ , \tag{10}$$

we can write the gyrokinetic equation as

$$\frac{\partial F}{\partial t} + \left[v_\parallel + \frac{q}{m} \frac{\underset{\sim}{E} \times \hat{\underset{\sim}{b}}}{\Omega} \right] \cdot \frac{\partial F}{\partial \underset{\sim}{R}} + \frac{q}{m} \underset{\sim}{E} \cdot \hat{\underset{\sim}{b}} \frac{\partial F}{\partial v_\parallel}$$

$$+ \underset{\sim}{v} \cdot \left[\left(\frac{\partial \rho}{\partial \underset{\sim}{x}} \right] \cdot \frac{\partial F}{\partial \underset{\sim}{R}} + \frac{\partial \mu}{\partial \underset{\sim}{x}} \frac{\partial F}{\partial \mu} + \frac{\partial v_\parallel}{\partial \underset{\sim}{x}} \frac{\partial F}{\partial v_\parallel} + \frac{\partial \phi}{\partial \underset{\sim}{x}} \frac{\partial F}{\partial \phi} \right]$$

$$+ \frac{1}{2} \frac{\partial}{B} \left(\frac{q}{m} \right)^2 \frac{\partial^2 f}{\partial \mu^2} \frac{\partial \bar{\Phi}^2}{\partial \phi} = 0. \tag{11}$$

The last term in Eq. (11) can be eliminated through gyrophase-averaging. Thus, this equation, which is the reduced form of Eq. (1), is amenable to the development of gyrokinetic particle simulation schemes for electrostatic as well as finite-β plasmas. In the following sections, our focus will be on the development of an electrostatic particle simulation scheme in the slab geometry. More general cases using Eq. (11) will be reported later.

III. Electrostatic Gyrokinetics in Slab

The gyrophase-averaged electrostatic gyrokinetic equation in the slab geometry can be obtained from Eq. (11) by neglecting the geometric terms, and it takes the form

$$\frac{\partial \langle F \rangle}{\partial t} + \underset{\sim}{v}_\parallel \cdot \frac{\partial \langle F \rangle}{\partial \underset{\sim}{R}} - \frac{q}{m} \left\langle \frac{1}{\Omega} \frac{\partial \Phi}{\partial \underset{\sim}{R}} \times \hat{\underset{\sim}{b}} \cdot \frac{\partial F}{\partial \underset{\sim}{R}} \right\rangle - \frac{q}{m} \left\langle \frac{\partial \Phi}{\partial \underset{\sim}{R}} \cdot \hat{\underset{\sim}{b}} \frac{\partial F}{\partial v_\parallel} \right\rangle = 0 \ , \tag{12}$$

where $\langle\ \rangle \equiv (2\pi)^{-1} \oint d\phi$. Let the electrostatic potential be

$$\Phi(\underset{\sim}{x}) = \sum_{\underset{\sim}{k}} \Phi(\underset{\sim}{k}) \exp(i\underset{\sim}{k} \cdot \underset{\sim}{x}) = \sum_{\underset{\sim}{k}} \Phi(\underset{\sim}{k}) \exp(i\underset{\sim}{k} \cdot \underset{\sim}{R} - i\underset{\sim}{k} \cdot \underset{\sim}{\rho}) , \tag{13}$$

and its gyrophase average becomes

$$\langle \Phi \rangle \equiv \langle \Phi \rangle_o = \sum_{\underset{\sim}{k}} \Phi(\underset{\sim}{k})\, J_o\left(\frac{k_\perp v_\perp}{\Omega}\right) \exp(i\underset{\sim}{k} \cdot \underset{\sim}{R}) , \tag{14}$$

in which

$$\langle \exp(\pm i\underset{\sim}{k} \cdot \underset{\sim}{\rho}) \rangle = J_o(k_\perp v_\perp/\Omega)$$

is used, and J_o is the Bessel function. From Eq. (9), the gyrophase-averaged distribution can be expressed as

$$\langle F \rangle = f + \frac{q}{m} \frac{\langle \Phi \rangle_o}{B} \frac{\partial f}{\partial \mu} . \tag{15}$$

Using the relation

$$\langle \exp[\pm i(\underset{\sim}{k}' + \underset{\sim}{k}'') \cdot \underset{\sim}{\rho}] \rangle = \sum_{n=\infty}^{\infty} J_n\left(\frac{k'v_\perp}{\Omega}\right) J_n\left(\frac{k''v_\perp}{\Omega}\right) \cos n\theta , \tag{16}$$

where $\theta = \cos^{-1}(\underset{\sim}{k}'_\perp \cdot \underset{\sim}{k}''_\perp / k'_\perp k''_\perp)$, the coupling term becomes

$$\langle \Phi\, \Phi \rangle = \langle \Phi \rangle_o \langle \Phi \rangle_o + 2 \frac{\partial \langle \Phi \rangle_1}{\partial \underset{\sim}{R}_\perp} \cdot \frac{\partial \langle \Phi \rangle_1}{\partial \underset{\sim}{R}_\perp} , \tag{17}$$

where only the first two leading term in Eq. (16) are kept and

$$\langle \Phi \rangle_1 = \sum_{\underset{\sim}{k}} \Phi(\underset{\sim}{k}) \frac{\underset{\sim}{k}_\perp}{k_\perp} J_1\left(\frac{k_\perp v_\perp}{\Omega}\right) \exp(i\underset{\sim}{k} \cdot \underset{\sim}{R}) \quad . \tag{18}$$

With the use of Eqs. (14) - (18), Eq. (12) reduces to

$$\frac{\partial \langle F \rangle}{\partial t} + \underset{\sim}{v}_\parallel \cdot \frac{\partial \langle F \rangle}{\partial \underset{\sim}{R}} - \frac{q}{m} \frac{1}{\Omega} \frac{\partial \langle \Phi \rangle_o}{\partial \underset{\sim}{R}} \times \hat{\underset{\sim}{b}} \cdot \frac{\partial \langle F \rangle}{\partial \underset{\sim}{R}} - \frac{q}{m} \frac{\partial \langle \Phi \rangle_o}{\partial \underset{\sim}{R}} \cdot \hat{\underset{\sim}{b}} \frac{\partial \langle F \rangle}{\partial v}$$

$$- \frac{q}{m} \frac{1}{\Omega} \frac{\partial}{\partial \underset{\sim}{R}} \left| \frac{\partial \langle \Phi \rangle_1}{\partial \underset{\sim}{R}_\perp} \right|^2 \times \hat{\underset{\sim}{b}} \cdot \frac{\partial}{\partial \underset{\sim}{R}} \left(\frac{q}{mB} \frac{\partial f}{\partial \mu} \right)$$

$$- \frac{q}{m} \frac{\partial}{\partial \underset{\sim}{R}} \left| \frac{\partial \langle \Phi \rangle_1}{\partial \underset{\sim}{R}_\perp} \right|^2 \cdot \hat{\underset{\sim}{b}} \frac{\partial}{\partial v_\parallel} \left(\frac{q}{mB} \frac{\partial f}{\partial \mu} \right) = 0 \quad . \tag{19}$$

Assuming f is Maxwellian in $v_\perp$, we found from Eq. (15)

$$f = \frac{\langle F \rangle}{1 - q\langle \Phi \rangle_o / T} \tag{20}$$

and

$$\frac{q}{mB} \frac{\partial f}{\partial \mu} = - \frac{q}{T} \frac{\langle F \rangle}{1 - q\langle \Phi \rangle_o / T} \quad . \tag{21}$$

Note that $\partial \langle \Phi \rangle_o / \partial \mu = 0$. Substituting Eq. (21) into Eq. (19), we obtain

$$\frac{\partial \langle F \rangle}{\partial t} + \underset{\sim}{v}_\parallel \cdot \frac{\partial \langle F \rangle}{\partial \underset{\sim}{R}} - \frac{q}{m} \frac{1}{\Omega} \left(\frac{\partial}{\partial \underset{\sim}{R}} \alpha \langle \Phi \rangle_o \right) \times \hat{\underset{\sim}{b}} \cdot \frac{\partial \langle F \rangle}{\partial \underset{\sim}{R}}$$

$$- \frac{q}{m} \left(\frac{\partial}{\partial \underset{\sim}{R}} \alpha \langle \Phi \rangle_o \right) \cdot \hat{\underset{\sim}{b}} \frac{\partial \langle F \rangle}{\partial v_\parallel}$$

$$- \left(\frac{q}{T}\right)^2 \frac{1}{(1-q\langle\Phi\rangle_0/T)^2} \frac{q}{m}\left(\frac{1}{\omega}\frac{\partial\langle\Phi\rangle_0}{\partial \underset{\sim}{R}} \times \hat{\underset{\sim}{b}} \cdot \frac{\partial}{\partial \underset{\sim}{R}} + \frac{\partial\langle\Phi\rangle_0}{\partial \underset{\sim}{R}} \cdot \hat{\underset{\sim}{b}} \frac{\partial}{\partial v_\parallel}\right) |\langle F\rangle| \left|\frac{\partial\langle\Phi\rangle_1}{\partial \underset{\sim}{R}_\perp}\right|^2 = 0 \quad , \tag{22}$$

where

$$\alpha = 1 - \frac{q}{T} \frac{1}{\langle\Phi\rangle_0 (1-q\langle\Phi\rangle_0/T)} \left| \frac{\partial \langle\Phi\rangle_1}{\partial \underset{\sim}{R}_\perp} \right|^2 .$$

This equation, which is totally independent of Φ, describes the evolution of the guiding center distribution $\langle F\rangle$ in terms of the gyrophase-averaged field quantities. The original distribution function F in Eq. (9) is related to $\langle F\rangle$ through Eqs. (15) and (21) as

$$F = \langle F\rangle - \frac{\langle F\rangle}{1-q\langle\Phi\rangle_0/T} \frac{q}{T} (\Phi - \langle\Phi\rangle_0) \quad . \tag{23}$$

The next step is to transform the field quantities from the guiding center coordinates $\underset{\sim}{R}$ back to the particle coordinates $\underset{\sim}{x}$. This transformation can be accomplished by performing the integration of $\oint d\phi \int_0^\infty v_\perp dv_\perp$ on Eqs. (22) and (23) and assuming

$$\langle F\rangle = \hat{F}(\underset{\sim}{R}, v_\parallel, t)\, f_m(v_\perp) \quad , \tag{24}$$

where f_m is Maxwellian in $v_\perp$ and homogeneous spatially. The multiple-scale particle simulation model,[14] which is the extension of the present scheme, has to be used to handle cases involving the perpendicular temperature gradient, i.e., $f_m = f_m(\underset{\sim}{R}, v_\perp)$. It is straightforward to carry out the integration for terms in Eqs. (22) and (23) involving neither $\langle\Phi\rangle_0$ nor $\langle\Phi\rangle_1$. For those with $\langle\Phi\rangle_0$ only, the integration yields

$$\tilde{\Phi}(\underset{\sim}{x}) = \sum_{\underset{\sim}{k}} \Phi(\underset{\sim}{k})\, \Gamma_o\left(k_\perp^2 v_t^2/\Omega^2\right) \exp(i\underset{\sim}{k}\cdot\underset{\sim}{x}) \quad , \tag{25}$$

where $v_t = (T/m)^{1/2}$ is the thermal velocity, and

$$\Gamma_o(b) = I_o(b)e^{-b} = \frac{1}{v_t^2}\int_o^\infty \exp\left(-v_\perp^2/2v_t^2\right) J_o^2\left(\frac{k_\perp v_\perp}{\Omega}\right) v_\perp dv_\perp \quad , \tag{26}$$

where $b = k_\perp^2 \rho_t^2 = k_\perp^2 v_t^2/\Omega^2$, I_o is the Bessel function. The integration of $\langle\Phi\rangle_o\langle\Phi\rangle_o$ and $\langle\Phi\rangle_1\langle\Phi\rangle_1$ can be carried out using Eq. (16), in which again only the two leading terms are kept, and the integrals of

$$\frac{1}{v_t^2}\int_o^\infty \exp\left(-\frac{v_\perp^2}{2v_t^2}\right) J_o^2\left(\frac{k_\perp' v_\perp}{\Omega}\right) J_o^2\left(\frac{k_\perp'' v_\perp}{\Omega}\right) v_\perp dv_\perp$$

$$= \sum_{n=o}^{\infty} \frac{(b')^n}{n!}\frac{\partial^n \Gamma_o(b')}{\partial(b')^n}\frac{(b'')^n}{n!}\frac{\partial^n \Gamma_o(b'')}{\partial(b'')^n} = \Gamma_o(b')\,\Gamma_o(b'') + b'b'' + \ldots, \tag{27}$$

$$\frac{1}{v_t^2}\int_o^\infty \exp\left(-\frac{v_\perp^2}{2v_t^2}\right) J_o\left(\frac{k_\perp' v_\perp}{\Omega}\right) J_1\left(\frac{k_\perp' v_\perp}{\Omega}\right) J_o\left(\frac{k_\perp'' v_\perp}{\Omega}\right) J_1\left(\frac{k_\perp'' v_\perp}{\Omega}\right) v_\perp dv_\perp$$

$$= \frac{1}{2}(b')^{1/2}(b'')^{1/2} - \frac{3}{4}(b')^{1/2}(b'')^{3/2} - \frac{3}{4}(b')^{3/2}(b'')^{1/2} + \ldots \quad , \tag{28}$$

and

$$\frac{1}{v_t^2}\int_o^\infty \exp\left(-v_\perp^2/2v_t^2\right) J_1^2\left(\frac{k_\perp' v_\perp}{\Omega}\right) J_1^2\left(\frac{k_\perp'' v_\perp}{\Omega}\right) v_\perp dv_\perp = \frac{1}{2} b'b'' + \ldots \quad , \tag{29}$$

where $b' = k_\perp'^2 \rho_t^2$ and $b'' = k_\perp''^2 \rho_t^2$. Consequently, the integration of Eq. (22) in ϕ and $v_\perp$ gives

$$\frac{\partial \tilde{F}}{\partial t} + v_{\parallel} \cdot \frac{\partial \tilde{F}}{\partial \underset{\sim}{x}} - \frac{q}{m} \frac{1}{c} \left(\frac{\partial}{\partial \underset{\sim}{x}} \tilde{\alpha} \tilde{\Phi} \right) \times \hat{\underset{\sim}{b}} \cdot \frac{\partial \tilde{F}}{\partial \underset{\sim}{x}} - \frac{q}{m} \left(\frac{\partial}{\partial \underset{\sim}{x}} \tilde{\alpha} \tilde{\Phi} \right) \cdot \hat{\underset{\sim}{b}} \frac{\partial \tilde{F}}{\partial v_{\parallel}} = 0 \quad , \tag{30}$$

where

$$\tilde{\alpha} = 1 - \frac{q}{T} \frac{\rho_t^2}{2} \left| \frac{\partial \tilde{\Phi}}{\partial \underset{\sim}{x}_{\perp}} \right|^2 / \tilde{\Phi}$$

and the integration of Eq. (23) in ϕ and $v_{\perp}$ as well as in $v_{\parallel}$ yields

$$\int F d\underset{\sim}{v} = n - \frac{q}{T} (\Phi - \tilde{\Phi}) (1 + \frac{q}{T} \tilde{\Phi}) n + (\frac{q}{T})^2 \rho_t^2 \left| \frac{\partial \Phi}{\partial \underset{\sim}{x}_{\perp}} \right|^2 n \quad , \tag{31}$$

where

$$n = \int_{-\infty}^{\infty} \tilde{F} (\underset{\sim}{x}, v_{\parallel}, t) \, dv_{\parallel} \quad . \tag{32}$$

Since the difference between the particle coordinates $\underset{\sim}{x}$ and the guiding-center coordinates $\underset{\sim}{R}$ vanishes after two gyrophase-averaging processes, the independent variables in Eq. (30) are now $\underset{\sim}{x}$, $v_{\parallel}$, t. The potentials $\Phi (\underset{\sim}{x})$ and $\tilde{\Phi} (\underset{\sim}{x})$ are defined by Eqs. (13) and (25), respectively. It should be pointed out here that the terms of the orders of $(k_{\perp}^2 \rho_t^2)^2 (q\Phi/T)^2$ and $(k_{\perp}^2 \rho_t^2) (q\Phi/T)^3$ have been neglected in obtaining Eqs. (30) and (31). Thus, the term $\Phi \tilde{\Phi}$ in Eq. (31) is accurate only to $k_{\perp}^2 \rho_t^2$. From Eqs. (31) and (32), Poisson's equation can then be written as

$$\nabla^2 \Phi - k_{Di}^2 \frac{n_i}{n_o} \left[(\Phi - \tilde{\Phi}) - \frac{\rho_i^2}{2} \nabla_{\perp}^2 \frac{e\Phi^2}{T_i} \right] = - 4\pi e (n_i - n_e), \tag{33}$$

where subscripts i and e denote species, $k_{Di}^2 = 4\pi e^2 n_o / T_i$ and n_o is the spatial

average of n_1. Here electron gyroradius effects are assumed to be small and neglected.

It is interesting to observe that the gyrokinetic equation, Eq. (30), in essence is a drift-kinetic equation with a gyrophase-averaged field $\tilde{\alpha}\,\tilde{\delta}$, and the second term on the left-hand side of Eq. (33) accounts for the polarization effects. Furthermore, $\hat{F}$, which is related to the phase-averaged quantity $\langle F \rangle$ in Eq. (24), is now the guiding-center distribution and n is the guiding-center density. Thus, the actual number density associated with the original distribution F consists of two parts, i.e., the guiding-center number density and the density due to polarization effects, as shown in Eq. (31). Equations (30), (32) and (33) form a convenient set of equations that can be used for the particle pushing. Moreover, since these equations are simply the usual gyrokinetic-Poisson system casting in a different form, they can also be used for analytical purposes. Contrary to the usual gyrokinetic formulation, the present scheme retains the gyroradius effects without the subsidiary ordering of the distribution function F. These equations are correct linearly for arbitrary values of $k_\perp \rho_t$ and nonlinearly for $k_\perp \rho_t < 1$. The inclusion of the gyroradius effects to the next order, i.e., $(k_\perp^2 \rho_t^2)^2\,(q\Phi/T)^2$, can easily be accomplished by retaining the corresponding terms in Eqs. (27) - (29) in the derivation. Since the resulting formulation is somewhat tedious, we prefer not to discuss it at the present time. The extension of the present scheme to include terms of the order of $(k_\perp^2 \rho_i^2)\,(q\Phi/T)^3$ and beyond requires the technique described in Ref. 14.

The definition of actual number density, Eq. (31), in the absence of the perturbed fields needs further discussion. Let's define

$$\hat{n}(\underset{\sim}{x}) = \int F \, d\underset{\sim}{v}$$

and

$$\hat{n}(\underset{\sim}{k}) = \frac{1}{L^3} \int F \exp(-i\underset{\sim}{k}\cdot\underset{\sim}{x})\, d\underset{\sim}{x}\, d\underset{\sim}{v} .$$

Since Jacobian, $J(\underset{\sim}{x},\underset{\sim}{v}/\underset{\sim}{R},\underset{\sim}{v})$, is unity in the slab geometry, the latter can be written as

$$\hat{n}(\underset{\sim}{k}) = \frac{1}{L^3} \int F \exp(-i\underset{\sim}{k}\cdot\underset{\sim}{R})\, \exp(+i\underset{\sim}{k}\cdot\underset{\sim}{\rho})\, d\underset{\sim}{R}\, d\underset{\sim}{v} . \tag{34}$$

From Eq. (23), $F = \langle F \rangle$ when $\Phi = \langle \Phi \rangle_o = 0$. Substituting Eq. (24) into Eq. (34) and carrying out the integration in $\underset{\sim}{v}$, we obtain

$$\hat{n}(\underset{\sim}{k}) = \frac{1}{L^3} \int n \exp\left(-\frac{k_\perp^2 \rho_t^2}{2}\right) \exp(-i\underset{\sim}{k}\cdot\underset{\sim}{R})\, d\underset{\sim}{R} , \tag{35}$$

where

$$\frac{1}{v_t^2} \int_0^\infty \exp\left(-\frac{v_\perp^2}{2v_t^2}\right) J_o\left(\frac{k_\perp v_\perp}{\rho}\right) v_\perp dv_\perp = \exp\left(-\frac{k_\perp^2 \rho_t^2}{2}\right)$$

has been used, and $n(\underset{\sim}{R}) = \int \bar{F}\, dv_\parallel$ is guiding center number density. For $k_\perp^2 \rho_t < < 1$ where $k_\perp$ describes the equilibrium variation, Eq. (35) gives

$$\hat{n}(\underset{\sim}{x}) = n + \frac{1}{2} \rho_t^2 \nabla_\perp^2 n . \tag{36}$$

Hence, the actual number density associated with the distribution function F should include the contribution from equilibrium density gradient. [For cases with a temperature gradient, i.e., for $f_m(\underset{\sim}{R},v_\perp)$, the contribution is $(1/2)\, \nabla_\perp^2 \rho_t^2 n$.] Accordingly, the ion guiding center number density n_i on the

right-hand side of Poisson's equation, Eq. (33), should be replaced by $\hat{n}_i(\underset{\sim}{x})$ in Eq. (36), and becomes

$$\text{RHS of Eq. (33)} = -4\pi e(n_i + \frac{1}{2}\rho_i^2 \nabla_\perp^2 n_i^{eq} - n_e). \tag{37}$$

Here n_i^{eq} represent the part of the ion guiding center number density when the perturbed fields are absent, whereas n_i is the total number density. The contribution of this additional term is usually very small and has been neglected in most analytical studies. However, for some cases in the particle simulation, its presence cannot be ignored because of the large density gradient used and the boundary conditions imposed for Poisson's equation.

IV Gyrokinetic Simulation Code and Results

As we have mentioned earlier, the resulting gyrokinetic equation, Eq. (30), resembles closely the usual drift-kinetic equation. Using the distribution function $\hat{F}$ in its discrete form,

$$\hat{F}(\underset{\sim}{x},v_\parallel,t) = \sum_{i=1}^{N} \delta[\underset{\sim}{x} - \underset{\sim}{x}_i(t)]\ \delta[v_\parallel - v_{\parallel i}(t)] \quad , \tag{38}$$

where N is the total number of particles of the particular species in the system, we obtain from Eq. (30) the equations of motion for the i-th particle:

$$\frac{d\underset{\sim}{x}_i}{dt} = \underset{\sim}{v}_{\parallel i} - \frac{q}{m}\frac{1}{\mathcal{D}}\frac{\partial(\tilde{\alpha}\tilde{\Phi})}{\partial \underset{\sim}{x}}\bigg|_{\underset{\sim}{x}_i,t} \times \hat{\underset{\sim}{b}} \tag{39}$$

$$\frac{dv_{\parallel i}}{dt} = -\frac{q}{m}\frac{\partial(\tilde{\alpha}\tilde{\Phi})}{\partial \underset{\sim}{x}}\bigg|_{\underset{\sim}{x}_i,t} \cdot \hat{\underset{\sim}{b}} \ ,$$

which are simply the characteristics of Eq. (30). They are the basic equations for our particle pushing and can be solved numerically using the usual predictor-corrector finite-difference scheme.[6] In the code, the ions are pushed with a modified potential of $\widetilde{\alpha\Phi}$, defined in Eqs. (25) and (30), while the electrons are acted upon by the original potential Φ. Since the particle gyration has been eliminated from the equations of motion, longer time-steps corresponding to the frequency of interest may be used in Eqs. (39). The additional constraint of $kv_t \Delta t < 1$ ordinarily does not pose any problem for our purposes. At every time step the number density is calculated by

$$n = \sum_{n=1}^{N} \delta[\underset{\sim}{x} - \underset{\sim}{x}_i(t)] \tag{40}$$

and is substituted into Poisson's equation, Eqs. (33) and (37), to determine Φ. The modified Poisson's equation without the α^2 term is in the form of an inhomogeneous Fredholm equation of the second kind in the Fourier $\underset{\sim}{k}$-space, and it can be solved readily using the method of successive approximations,[15] with the constraint that number density associated with the polarization effects is conserved. The small nonlinear term can be included perturbatively. The determination of n_i^{eq} in Eq. (37) is somewhat difficult due to particle diffusion during the course of the simulation. However, it can be approximated by taking the mean of the spatial averages of electron and ion number densities in the homogeneous directions, i.e.,

$$n_i^{eq} = \langle n_i + n_e \rangle_{homo.}/2 \quad .$$

This ambiguity can be removed in the multiple scale particle simulation

model.[14]

The gyrokinetic particle simulation scheme has been implemented in a two-and-one-half dimensional (x,y,v_x,v_y,v_z) code in the slab geometry. To simplify its algorithm we have dropped all of the nonlinear terms in Φ, i.e., $\tilde{\alpha} = 1$ in Eq. (39) and $\rho_i^2 \nabla_\perp^2 \Phi^2 = 0$ in Eq. (33). The simulation plasma is bounded by two conducting walls in the x direction where the potential Φ vanishes and the simple reflecting condition is imposed for the particles hitting the wall. The periodic condition is used for both the waves and the particles in the y direction. The magnetic field is in the y-z plane where $B_z \gg B_y$. In the case of shear, B_y is a function of x. The inhomogeneity exists only in the x direction with a constant κ $(= -n'/n)$. Two cases, one with shear and the other without, have been studied using the code. The results agree very well in every aspect of the instability with those obtained from the code which uses exact dynamics for the ions and guiding center approximation for the electrons.[6]

Case 1

This is a shearless case. Using the grid size Δ as a basic unit, the simulation parameters are

$$L_x \times L_y = 64\Delta \times 32\Delta,\ n_o = 16/\Delta^2,\ m_i/m_e = 1837\ ,$$

$$T_e/T_i = 9,\ \omega_{ce}/\omega_{pe} = 10,\ \lambda_{De}/\Delta = 1.5,\ \text{particle size}/\Delta = 1.5\ ,$$

$$B_y/B_z = 0.0053,\ \rho_i/\Delta = 2.14,\ \kappa\rho_i = 0.15,$$

$$k_y\rho_i = 0.428m,\ \omega^*/\omega_{pe} = 0.00315m,\ \text{where } m = 0, \pm 1, \pm 2, \ldots$$

The simulation has been carried out with $\omega_{pe}\Delta t = 80$ using the gyrokinetic code. The time evolution of $e\phi/T_e$ for the most unstable $m = 1$ mode measured at the middle of the plasma in x and the corresponding frequency spectra are shown in Fig. 1.[16] Simulation results from the previous code[6] with $\omega_{pe}\Delta t = 15$ are shown in Fig. 2. The agreement between the two is excellent in terms of the linear frequency and growth rate, the saturation amplitude and the nonlinear frequency shift. The higher saturation amplitude in the gyrokinetic code is probably caused by the absence of nonlinear ϕ^2 terms. As we can see, the simulation plasma is much quieter in the gyrokinetic code because of the elimination of the ion gyromotion. Thus, we can afford to use fewer particles and milder density gradient in the simulation. It should also be mentioned here that the observed linear properties of the instability agree with the theory.[12] The nonlinear saturation and the frequency shift are mainly the result of the mode coupling processes.[17] The effect of n_i^{eq} in Eq. (37) on the instability is insignificant in this case.

Case 2

In this case, shear is included and the magnetic field is described by

$$\underset{\sim}{B} = B_o(\hat{\underset{\sim}{z}} + \hat{\underset{\sim}{y}}\, x/L_s) \quad ,$$

where L_s is the shear scale length. The rational surface $x = 0$ is located at the left-hand boundary of the system. Therefore, we only allow odd modes in the simulation. The other parameters are

$$L_x \times L_y = 64\Delta \times 32\Delta,\ n_o = 1.6/\Delta^2,\ m_i/m_e = 100,$$

$T_e/T_i = 1$, $\omega_{ce}/\omega_{pe} = 10$, $\lambda_{De}/\Delta = 2.5$, particle size/$\Delta$ = 1.5 ,

$\rho_i/\Delta = 2.5$, $\kappa\rho_i = \rho_i/L_n = 0.175$, $L_s/L_n = 56$,

$k_y \rho_i = 0.5m$, $\omega^*/\omega_{pe} = 0.00875m$, where $m = 0, \pm 1, \pm 2, \ldots$

The time step in the gyrokinetic code is $\omega_{pe} \Delta t = 40$, and the term associated with n^{eq} in Eq. (57) is also included. Figure 3 shows the results for the most unstable m = 1 mode where the time evolution of $e\Phi/T_e$ at $x/\Delta = 25$ and the mode structure for $\omega/\omega^* = 0.7$ are given. The corresponding results from the previous code with $\omega_{pe}\Delta t = 4$ are shown in Fig. 4. In both cases a band-pass filter with the width of ω^* has been applied to eliminate the numerical noise in $e\Phi/T_e$. The mode structures are obtained through the use of the two-point-spatial correlation function.[13] Again, the two results are very similar. The nature of the instability, which is not a bona fide eigenmode, has been discussed in Ref.13. When the term involving n_i^{eq} is not included in the gyrokinetic simulation, somewhat different results have been obtained. In this case, the frequency is lower, $\omega/\omega^* = 0.5$, and the saturation amplitude is also lower, $e\Phi/T_e = 4\%$. Apparently, the ambipolar potential arising from n_i^{eq} has played a part in the instability.

From the two cases studied here, one can conclude that the gyrokinetic code can indeed reproduce all the relevant physics in drift instabilities with considerable saving in computing resources. The time-steps used in these two codes show a gain of a factor of 5 ~ 10. Compared with the conventional codes where exact dynamics is preserved for both electrons and ions and the time-step is limited by $\omega_{pe} \lesssim 0.2$, the gain can be as high as 2 ~ 3 orders of magnitude. Moreover, the simulation plasma is much quieter which makes the interpretation and the understanding of the results much easier.

Conclusions

We have presented in this paper a new scheme for particle simulation based on the gyrokinetic approach. A 2-1/2-dimensional electrostatic code in the slab geometry utilizing the scheme has given satisfactory results. There are numerous advantages in using this code for studying microinstabilities - long time-step being one of them. In conjunction with the multiple-scale model,[14] the code can be used to study the phenomena associated with steady state drift turbulence such as anomalous particle and energy diffusion. Its extension to a fully 3-dimensional code similar to those in Ref. 7 should be straightforward. The procedures given in Sec. III also serve as a guide for the development of comparable schemes for simulating electrostatic and low-β plasmas in the toroidal geometry. The assumption, that the distribution function is Maxwellian in $v_\perp$ leading to Eqs. (30) and (33), can probably be removed by performing the second gyrophase-averaging numerically. Such a scheme has yet to be devised. Better still, if one could obtain an efficient particle simulation scheme based on Eqs. (11) or (12) alone without the prior gyrophase-averaging processes, arbitrary values of $k_\perp \rho_i$ could then be preserved in the nonlinear dynamics.

Acknowledgments

The author wishes to thank Dr. W. M. Tang, Dr. L. Chen, and Dr. F. W. Perkins for their continuing interest in this work and their helpful comments. Discussions with Dr. C. Oberman and Dr. P. Catto are also gratefully acknowledged.

This work is supported by the U.S. Department of Energy Contract No. DE-AC02-CHO-3073.

References

[1] RUTHERFORD, P. H., and FRIEMAN, E. A., Phys. of Fluids 11, 569 (1968).

[2] TAYLOR, J. B., and HASTIE, R. J., Plasma Phys. 10, 479 (1968).

[3] CATTO, P. J., Plasma Phys. 20, 719 (1978).

[4] CHENG, C. Z., and OKUDA, H., Phys. Rev. Lett. 38, 708 (1977).

[5] LEE, W. W., CHANCE, M. S., and OKUDA, H., Phys. Rev. Lett. 46, 1675 (1981).

[6] LEE, W. W., and OKUDA, H., J. Comput. Phys. 26, 139 (1978).

[7] CHENG, C. Z., and OKUDA, H., J. Comput Phys. 25, 133 (1977).

[8] LEE, W. W., OKUDA, H., and NEVINS, W. M. (in preparation).

[9] MASON, R. J. (to apear in J. Comput. Phys.).

[10] DENAVIT, J. (to appear in J. Comput. Phys.).

[11] FRIEDMAN, A., LANGDON, A. B., and COHEN, R. T., UCRL-86291, Lawrence Livermore National Laboratory, Livermore, CA (1981).

[12] LEE, W. W., KUO, Y. Y., and OKUDA, H., Phys. Fluids 24, 617 (1978).

[13] LEE, W. W., NEVINS, W. M., OKUDA, H., and WHITE, R. B., Phys. Rev. Lett. 43, 347 (1979).

[14] LEE, W. W., and CHEN, L. (in preparation).

[15] See for example, I. Stakgold, Boundary Value Problems of Mathematical Physics (MacMillan, New York, 1967), Vol. 1.

[16] The diagnostic package ZED by W. M. Nevins has been used to obtain the data given here.

[17] LEE, W. W., TANG, W. M., CHENG, C. Z. and CHEN, L., Bull Am. Physc. Soc. 26, 1012 (1981).

Figure Captions

Fig. 1. Time evaluation of $e\Phi/T_e$ for the m = 1 mode and the corresponding frequency spectrum (measured at the middle of the system in x) using the gyrokinetic code.

Fig. 2. Time evolution of $e\Phi/T_e$ for m = 1 mode and the corresponding frequency spectrum (measured at the middle of the system in x) using the previous code.

Fig. 3. Time evolution of $e\Phi/T_e$ for the m = 1 mode at $x/\Delta = 25$ and the corresponding mode structure for $\omega/\omega^* = 0.7$ using the gyrokinetic code.

Fig. 4. Time evolution of $e\Phi/T_e$ for m = 1 mode at $x/\Delta = 25$ and the corresponding mode structure for $\omega/\omega^* = 0.7$ using the previous code.

#81T0258

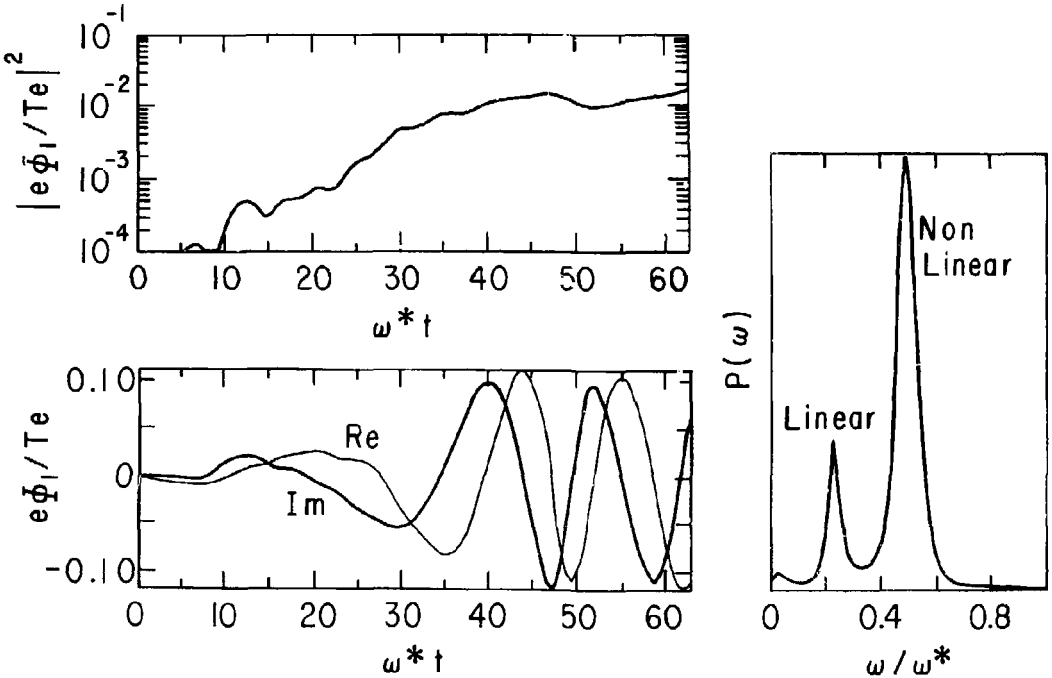

Fig. 1

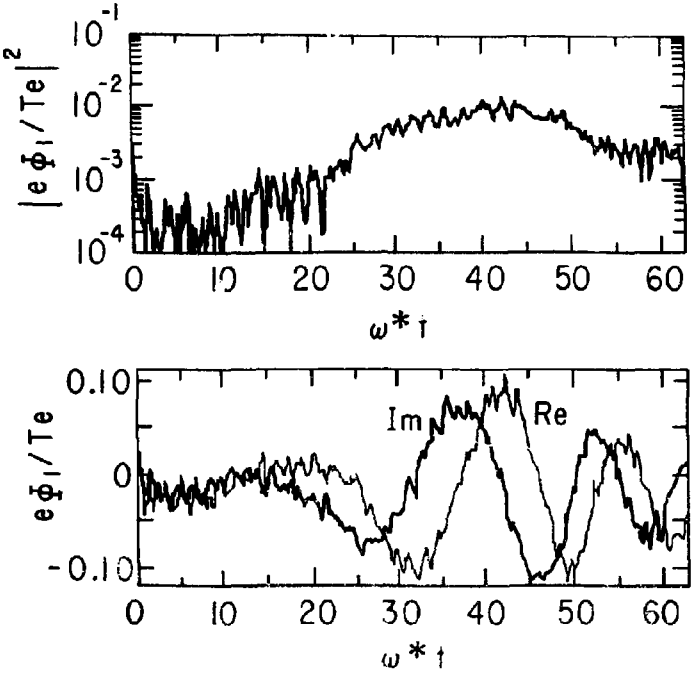
$|e\phi_1/Te|^2$
10^{-1}
10^{-2}
10^{-3}
10^{-4}
0
10
20
30
40
50
60
$\omega^* t$
$e\phi_1/Te$
0.10
0
-0.10
Im
Re
0
10
20
30
40
50
60
$\omega^* t$

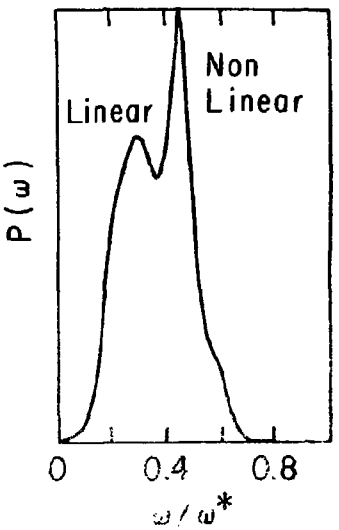
P(ω)
Linear
Non Linear
0
0.4
0.8
ω/ω^*

FIG. 2

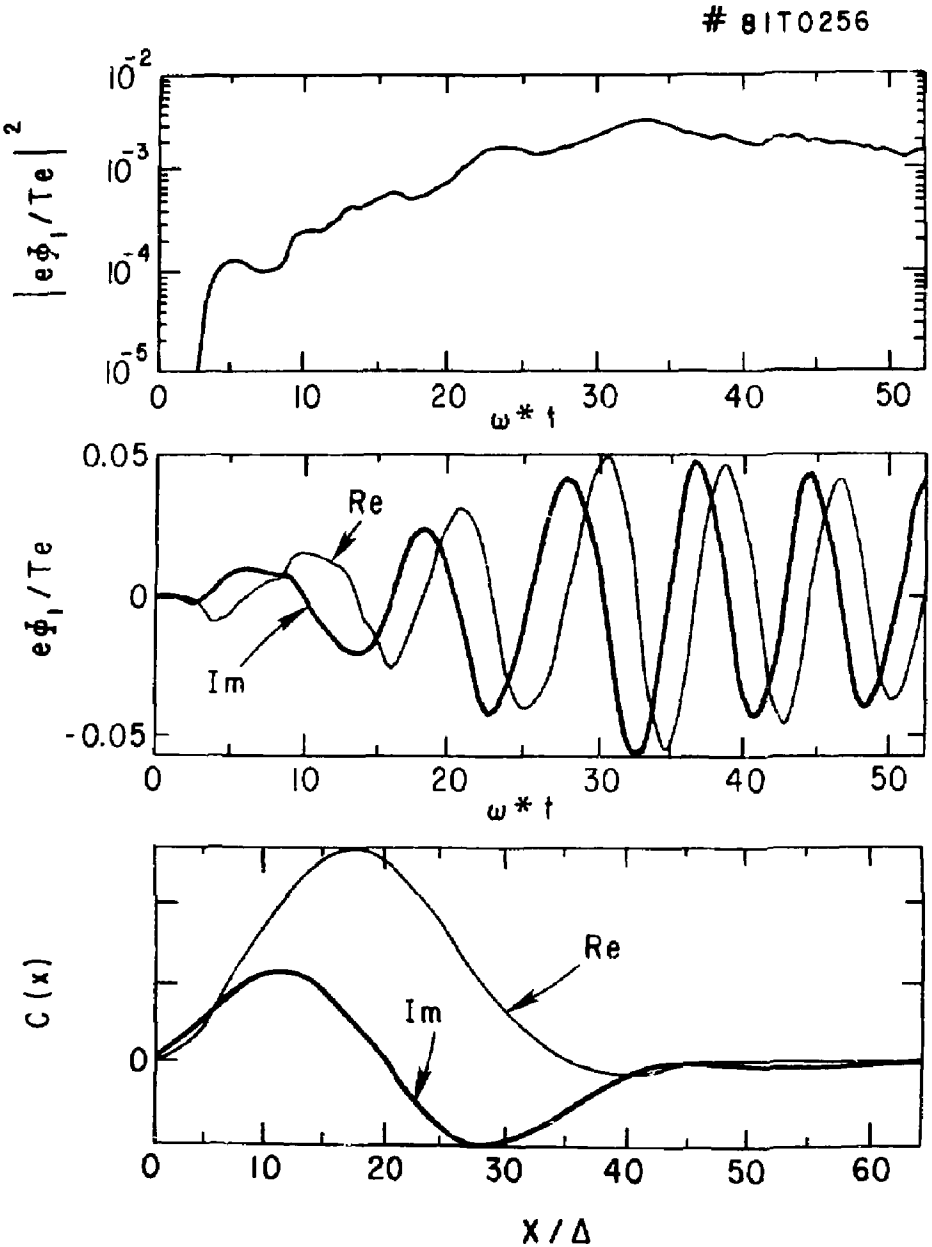
81T0256
10^{-2}
10^{-3}
10^{-4}
10^{-5}
$|e\phi_1/Te|^2$
0
10
20
30
40
50
ω * t
0.05
0
-0.05
$e\phi_1/Te$
Re
Im
0
10
20
30
40
50
ω * t
C(x)
Re
Im
0
0
10
20
30
40
50
60
X / Δ

Fig. 3

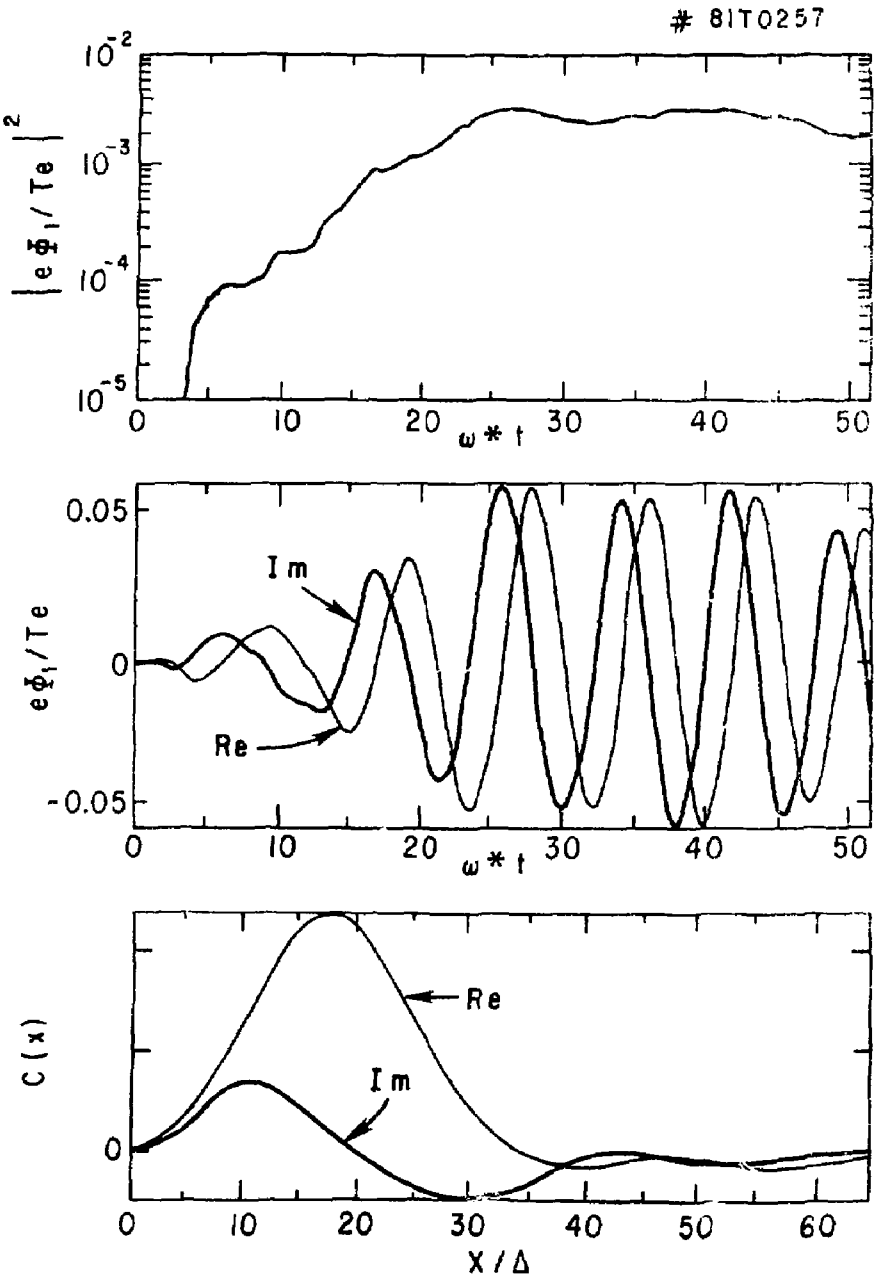
81T0257
10^{-2}
10^{-3}
10^{-4}
10^{-5}
$|e\Phi_1/Te|^2$
0
10
20
30
40
50
$\omega * t$
0.05
0
-0.05
$e\Phi_1/Te$
Im
Re
$\omega * t$
C(x)
Re
Im
0
10
20
30
40
50
60
X/Δ

Fig. 4